Histochem Cell Biol
DOI 10.1007/s00418-014-1203-4

ORIGINAL PAPER

Application perspectives of localization microscopy in virology

C. Cremer · R. Kaufmann · M. Gunkel · F. Polanski · P. Müller · R. Dierkes · S. Degenhard · C. Wege · M. Hausmann · U. Birk

Accepted: 20 February 2014

Abstract Localization microscopy approaches allowing an optical resolution down to the single-molecule level in fluorescence-labeled biostructures have already found a variety of applications in cell biology, as well as in virology. Here, we focus on some perspectives of a special localization microscopy embodiment, spectral precision distance/position determination microscopy (SPDM). SPDM permits the use of conventional fluorophores or fluorescent proteins together with standard sample preparation conditions employing an aqueous buffered milieu and typically monochromatic excitation. This allowed super-resolution imaging and studies on the aggregation state of modified tobacco mosaic virus particles on the nanoscale with a single-molecule localization accuracy of better than 8 nm, using standard fluorescent dyes in the visible spectrum. To gain a better understanding of cell entry mechanisms during influenza A virus infection, SPDM was used in conjunction with algorithms for distance and cluster analyses to study changes in the distribution of virus particles themselves or in the distribution of infection-related proteins, the hepatocyte growth factor receptors, in the cell membrane on the single-molecule level. Not requiring TIRF (total internal reflection) illumination, SPDM was also applied to study the molecular arrangement of gp36.5/m164 glycoprotein (essentially associated with murine cytomegalovirus infection) in the endoplasmic reticulum and the nuclear membrane inside cells with single-molecule resolution. On the basis of the experimental evidence so far obtained, we finally discuss additional application perspectives of localization microscopy approaches for the fast detection and identification of viruses by multi-color SPDM and combinatorial oligonucleotide fluorescence in situ hybridization, as well as SPDM techniques for optimization of virus-based nanotools and biodetection devices.

C. Cremer (✉) · U. Birk
Institute of Molecular Biology (IMB), 55128 Mainz, Germany
e-mail: c.cremer@imb-mainz.de;
cremer@bmm.uni-heidelberg.de

C. Cremer · F. Polanski
Institute of Pharmacy and Molecular Biotechnology (IPMB), University Heidelberg, 69120 Heidelberg, Germany

C. Cremer · M. Gunkel · P. Müller · M. Hausmann · U. Birk
Kirchhoff Institute for Physics (KIP), University Heidelberg, 69120 Heidelberg, Germany

C. Cremer · U. Birk
Department of Physics, University of Mainz, 55128 Mainz, Germany

R. Kaufmann
Division of Structural Biology, Wellcome Trust Centre for Human Genetics, Oxford, UK

R. Kaufmann
Department of Biochemistry, University of Oxford, Oxford, UK

M. Gunkel
BioQuant Center, University Heidelberg, 69120 Heidelberg, Germany

R. Dierkes
Institute of Molecular Virology, Westfälische Wilhelms-Universität Münster, 48149 Münster, Germany

S. Degenhard · C. Wege
Institute of Biology, University of Stuttgart, 70550 Stuttgart, Germany

Published online: 11 March 2014

Keywords Nanoscopy of viruses · Superresolution · Single-molecule localization microscopy · SPDM · Virus-based biosensing

Introduction

Viral infections cause a large number of major diseases in man, from influenza to small pox, Hepatitis and AIDS, or certain types of cancer; they pose health problems on the global scale, with hundreds of millions of infections annually. Furthermore, viruses are involved in various animal and plant diseases of high economic impact. On the other hand, stable viral or virus-like nanoparticles, especially of plant or bacterial origin, have gained increasing importance as multivalent scaffolds for nanotechnology and diagnostics during recent years. Loaded with active molecules or contrast agents, they are being tested for applications, e.g., in biosensing devices or as versatile nanocarriers for tumor imaging and drug delivery in vivo [for an actual overview, refer to, e.g., (Bittner et al. 2013)].

While the development of well-corrected high numerical aperture microscopes in the second half of the nineteenth century made possible to readily identify bacteria, most viruses appeared to be invisible units. This changed only with the advent of electron microscopy (EM) many decades later, which demonstrated the diminutive dimensions of these entities: The typical size of viruses was found to be in the order of 50–100 nm, and hence considerably below the conventional, diffraction caused limit of resolution of visible light microscopy of about 200 nm. EM analyses provide images of viruses with an optical resolution down to few nm; making possible a detailed study of their morphology and interaction with their hosts or of the integrity of viral nanoparticles in preparations adapted to diverse in- and ex-vivo applications. On the other side, such EM analyses require a fairly high workload in specimen preparation; due to harsh fixation conditions, it is impractical to use EM to monitor viral-cell interactions in vivo or to visualize small functional molecules interlinked with virus-derived templates. Another problem in EM studies is the difficulty to separately identify multiple molecule types simultaneously. Consequently, it should be highly desirable to develop (far field) light optical approaches with enhanced resolution.

Until recently, from the methodological side, this goal was regarded to be excluded by the fundamental laws of physics: For about a hundred years, it was generally accepted that the limits to the optical resolution of the light microscope stated by Abbe (1873) and Rayleigh (1896) of about half the wavelength of the light used for observation, or about 200 nm in the object plane, were not surmountable, due to the very nature of light. In the last two decades, however, new developments in photophysics and optical technology have made it possible to realize various far-field fluorescence microscopy techniques by which the conventional resolution limits have been substantially circumvented. This revolution was achieved by applying optical conditions not subject to the specific conditions of the Abbe/Rayleigh theories [for reviews, see (Cremer 2012; Cremer and Masters 2013; Hell 2007, 2009)]. For example, using stimulated emission depletion microscopy (STED) based on a focused scanning approach, an optical resolution of cellular structures in the 15 nm range was realized (Donnert et al. 2006). Visualization of the viral envelope (Env) glycoprotein distribution on the surface of individual human immunodeficiency virus type 1 (HIV-1) particles with stimulated emission depletion (STED) superresolution fluorescence microscopy (Chojnacki et al. 2012) thus revealed maturation-induced clustering of Env proteins that depended on interaction of the Env-tail with the main viral structural polyprotein Gag.

Another ‘superresolution’ or ‘nanoscopy’ approach denoted as patterned excitation or structured illumination microscopy (PEM/SIM) (Gustafsson 2000; Heintzmann and Cremer 1999; Heintzmann and Gustafsson 2009; Schermelleh et al. 2008) achieved an optical resolution (object plane) in the 100-nm range by using a structured pattern of the light distribution instead of the conventional homogeneous illumination; axially structured illumination methods allowed to measure the extent of small fluorescent-labeled structures along the optical axis down to sizes in the few tens of nm range, also in 3-D-conserved nuclei (Albrecht et al. 2001, 2002; Baddeley et al. 2007, 2010; Hildenbrand et al. 2005; Reymann et al. 2008).

In addition to scanning and structured/patterned-illumination-based nanoscopy approaches, various methods of spectrally assigned localization microscopy (SALM) techniques [often abbreviated as single-molecule localization microscopy (SMLM) or ‘localization microscopy’] have been conceived and realized to study biostructures with an optical resolution down to the few nm scale.

Generally, the SALM techniques are based on the independent registration of the diffraction images (‘optical isolation’) produced by point emitters, using appropriate differences in their ‘spectral signatures’ in conjunction either with near-field microscopy (Betzig 1995; Ha et al. 1996), or with far-field fluorescence microscopy systems (Cremer et al. 1998, 1999). For example, differences in the absorption/emission spectrum of photostable fluorophores (Van Oijen et al. 1998; Bornfleth et al. 1998; Esa et al. 2000, 2001; Rauch et al. 2000, 2008); or differences in the time domain, such as variations in fluorescence life times (Heilemann et al. 2002); or the time-dependent stochastic switching of fluorescence emission characteristics (Baddeley et al. 2009, 2011; Bates et al. 2007; Betzig et al. 2006; Bock et al. 2007; Fölling et al. 2008; Heilemann

et al. 2008; Hess et al. 2006; Huang et al. 2008; Lemmer et al. 2008, 2009; Lidke et al. 2005; Löschberger et al. 2012; Reymann et al. 2008; Rust et al. 2006; Shroff et al. 2008; Shtengel et al. 2009; Steinhauer et al. 2008) have been used for optical isolation of 'point emitters'. In this way, it became possible to assign the center/maximum of the diffraction images independently from each other with an accuracy down to a small fraction of the pixel size of the detector; due to the design of the optical instrument, the center coordinates thus determined can be correlated with the position of the point emitter in the object plane; hence, distances substantially smaller than the conventional resolution limit can be measured, even if far-field fluorescence microscopy systems with homogeneous excitation are used (Cremer et al. 1998, 1999). In the case of the Rayleigh/Abbe criterion (smallest detectable distance between two neighboring point sources), this enhancement in optical resolution is limited only by the localization accuracy σ_{loc} of the optically isolated point emitters; σ_{loc} itself is dependent on various parameters of the optical system used, the background noise, or the number of fluorescence photons registered from a given point source (Bornfleth et al. 1998). Experimentally, σ_{loc} values down to the subnanometer range have been reported (Albrecht et al. 2001; Pertsinidis et al. 2010; Schmidt et al. 2000), using excitation wavelengths in the 500–700 nm range. In case the Nyquist criterion has to be applied to elucidate nanostructural detail, in addition to the localization accuracy σ_{loc}, the density ρ_{em} of optically isolated point emitters becomes important. To enhance ρ_{em}, the SALM methods for stochastic photoswitching referred to above have been especially useful to image cellular nanostructures down to the single-molecule resolution level (for reviews, see Cremer et al. 2011; Cremer and Masters 2013; Hess et al. 2009; Müller et al. 2012; Van de Linde et al. 2011; Zhuang 2009).

A particular feature of the special SALM-technique 'spectral precision distance/position determination microscopy' (SPDM) applied here is the possibility to use conventional green fluorescent proteins/organic fluorophores and mild standard preparation conditions (including physiological ones), together with photoswitching/readout by a single laser frequency for a given molecule type. Like the other localization microscopy techniques mentioned, SPDM is generally based on the principle of optical isolation of fluorescent point emitters (e.g., molecules) by using different 'spectral signatures' for discrimination. In the original SPDM concept (Cremer et al. 1998, 1999), in addition to differences in the excitation/absorption spectra of photostable fluorophores (Bornfleth et al. 1998; Esa et al. 2000, 2001), these signatures included time-dependent changes in the fluorescence emission such as different fluorescence life times (Heilemann et al. 2002) as well as random labeling approaches (Cremer et al. 2003). On these principles, an advanced SPDM method ('SPDM with physically modified fluorophores/SPDM$_{Phymod}$', in the following abbreviated as SPDM) was realized which allowed an efficient optical isolation of individual standard synthetic fluorophores in cellular structures at high molecule densities, using the same laser frequency for both photoswitching, fluorescence excitation and bleaching of a given molecule type, in combination with standard preparation conditions (Reymann et al. 2008; Lemmer et al. 2008). In contrast to the original 'Stochastic Optical Reconstruction' (STORM) method (Rust et al. 2006), instead of pairs of molecules and different laser frequencies, optical isolation by 'blinking' is possible also with single molecules. In this respect, SPDM is related to the direct STORM (dSTORM) and similar techniques published shortly after Reymann et al. 2008 (Heilemann et al. 2008; Steinhauer et al. 2008; Fölling et al. 2008) There remain, however, many differences between the actual dSTORM/SPDM protocols (Cremer and Masters 2013). The SPDM method has already been successfully applied in the analysis of nuclear pore complex distribution (Reymann et al. 2008); of protein distributions and specific DNA sequences in the cell nucleus (Gunkel et al. 2009; Kaufmann et al. 2009; Weiland et al. 2011); of membrane proteins, such as the analysis of breast cancer-related Her2/neu clusters (Kaufmann et al. 2011); of claudin networks (Kaufmann et al. 2012); of glycoproteins (Huber et al. 2012); of the expression of viral proteins (Müller et al. 2014); of the morphology of tobacco mosaic viruses in aqueous suspensions (Cremer et al. 2011); or in the analysis of influenza virus infection with respect to the spatial distribution of hepatocyte growth factor receptors (HGFR) membrane proteins (Wang et al. 2014).

In this contribution, we shall first present the state of the art of our localization microscopy/SPDM-based analyses related to virus particle morphology and aggregation in aqueous solution; to virus-cell interaction and to viral protein expression. In previous contributions (Cremer et al. 2011; Wang et al. 2014; Müller et al. 2014, methodological details of these SPDM applications have been described. Here, we focus on the impact of superresolution microscopy on virology. We shall first summarize the state of the art, including some hitherto unpublished material. Based on this experience, we shall then discuss some perspectives for use of localization-based superresolution microscopy in this field, including the possibility to identify a large variety of viruses by multi-color SPDM and combinatorial oligonucleotide fluorescence in situ hybridization (COMBO-FISH, Hausmann et al. 2003; Müller et al. 2010), and to analyze critical parameters of plant viral nanoparticle preparations for technical and medical applications, such as aggregate formation in suspension or surface distribution of

molecules coupled to tobacco mosaic virus (TMV) nucleoprotein biotemplates (Geiger et al. 2013).

Material and methods

Localization microscopy/SPDM

SPDM setup

The SPDM setup used has been described in detail previously (Cremer 2012; Gunkel et al. 2009; Kaufmann et al. 2009; Lemmer et al. 2008; Reymann et al. 2008). Briefly, a diode-pumped solid-state (DPSS) laser with a wavelength of 488 nm (Sapphire HP488, Coherent, Dieburg, Germany) was utilized for excitation of antibody bound Alexa488 fluorescent molecules, of Atto488 fluorescent molecules, and of yellow fluorescent protein (eYFP) (for details see Reymann et al. 2008; Lemmer et al. 2008; Gunkel et al. 2009; Cremer et al. 2011). The specimens were illuminated by the defocused laser beam (object plane diameter several tens of μm) using a high numerical aperture objective lens (63×/NA1.4 oil). The fluorescence light was transmitted through a dichroic mirror and an emission filter and then imaged via a lens with a magnification of 1.0× onto a highly sensitive CCD camera with low readout/multiplicative noise (SensiCam QE, PCO Imaging, Kehlheim, Germany).

Data acquisition, position determination and visualization

To obtain an SPDM image with enhanced resolution, typically one to several thousand frames (fr) of the same region of interest of the same object were taken at a rate of ca. 10 fr/s, using an illumination intensity of about 25 kW/cm^2. The electron counts for each pixel of the CCD camera were converted to photon numbers in each image of the data stack. Differential image data were calculated by subtracting the succeeding from the preceding frame. Only a few fluorescent signals were visible in each frame; thus, we assumed that each signal contained fluorescent light from a single molecule. By fitting a two-dimensional Gaussian with a linear estimation of the background noise to single-molecule signals, the positions of the registered molecule signals were determined (Kaufmann et al. 2009). All the positions found were assigned to a single localization map, i.e., a list of coordinates together with values for photon count number of signal and background and for localization accuracy.

For visualization of the position data assigned to the localization map, various image representations were generated (Kaufmann et al. 2009, 2011, 2012). By blurring the position of each individual molecule signal with the individual localization accuracy, an image of the localization map was generated. The width of the blur kernel corresponds to the optical, single-molecule resolution in the reconstructions: Two adjacent, blurred molecule signals in a distance $d_{\min}$ still visually separated from each other indicated a similar (two-point) optical resolution valid for fluorescent point emitters according to the Rayleigh criterion (Rayleigh 1896). This means that any fluorescent molecule positions in the specimen with a mutual distance larger than $d_{\min}$ can be discriminated from each other and assigned to a localization map. Such a two-point resolution may provide substantial biologically relevant information even in the case that only a few molecules can be localized within a diffraction limited area given by the conventional resolution limit (Esa et al. 2000, 2001; Rauch et al. 2000, 2008). To obtain a visualization of the structural resolution achieved (Cremer and Masters 2013), the localization map was rendered by the density of the detected molecules and the localization accuracy. Blurring each molecule position with a Gauss kernel corresponding to the distance to the next neighboring molecule(s) generates an image with a resolution dependent on the local molecule densities (termed density rendered image, Kaufmann et al. 2012). In the experiments reported here, the mean estimated localization accuracy was typically around 20 nm for cellular specimens and 8 nm for tobacco mosaic virus (TMV), excitation at wavelength $\lambda_{exc} = 488$ nm. While the density rendered image facilitates the visual inspection of structural details and the localization accuracy blurred image depicts the precision of the detected single-molecule positions, the unblurred localization map makes possible a detailed quantitative analysis, such as counting of individual molecule signals, distance frequency distributions, accumulations into clusters, comparison with random distributions. In this report, all analyses and conclusions are based on the direct evaluation of the original localization map, taking into account the limits in (optical and structural) resolution obtained.

Data analysis

The localization maps of the positions of single-molecule signals obtained were analyzed by a variety of evaluation tools described in detail elsewhere (Kaufmann et al. 2009, 2011, 2012). In particular, normalized frequencies were calculated from the SPDM map positions for the distance distribution of reporter molecules on the membrane. To identify aggregations of molecules, a density-based cluster definition was used. Here, a cluster was defined as an ensemble of molecules where around each molecule signal, three or more neighboring signals were counted within a distance $r = 60$ nm. This means that all molecules that had at least three neighbors within a distance of 60 nm were assigned to the same cluster. Consequently, also larger or

smaller cluster sizes than 2r can be obtained. The number of molecule signals within a given cluster is referred to as N_{CL}.

For comparison, random distributions of points were generated with the same mean density as the localization data. In order to keep the possibility of clustering in the random distribution of points lower, a critical density was introduced to reject clusters with densities below that value, i.e., clusters present based on pure statistics. For further details, see (Gunkel et al. 2009; Kaufmann et al. 2011).

Preparation of fluorescently labeled plant-derived TMV

Rod-shaped, genetically engineered TMV particles exposing an amino group (TMV_{Lys}) on every of their ~2,100 coat protein (CP) subunits (Geiger et al. 2013) were propagated in and isolated from *Nicotiana tabacum 'Samsun' nn plants* (Mueller et al. 2010). Covalent labeling of their CPs via the NH_2 groups followed a 'click chemistry' mode with tenfold molar excess of Atto488 succinimidyl (NHS) ester (Sigma-Aldrich, München, Germany) in relation to the CP number, in 10 mM sodium potassium phosphate (SPP) buffer pH 7.4. A 100 µl reaction mixture with 100 µg TMV and an appropriate amount of dye-NHS ester was shaken at 600 rpm (Thermomixer Compact, Eppendorf, Hamburg, Germany) and 20 °C for 1.5 h in the dark. Unbound excess dye was separated from the TMV rods by ultracentrifugation (2 h, 15 °C, 120,000*g*; Sorvall Ultra Pro 80, Thermo Fisher Scientific Inc., Waltham, USA) and discarded with the supernatant. The pellet of modified virus derivatives was washed twice by re-suspension in 10 mM SSP pH 7.2 and re-sedimentation. The labeling efficiency was determined via UV absorption spectroscopy (NanoDrop ND-1000, PEQLAB Erlangen, Germany) to about 40 % of the viral CP subunits of the sedimented TMV tubes, corresponding to about 840 individual dye molecules per 300 nm length of a single monomeric viral particle. Atto488-labeled TMV was diluted to 0.1 pg/µl in water; 5 µl were placed on a microscope slide (Menzel, Braunschweig, Germany) and subjected to a vacuum until the liquid was evaporated.

Preparation of influenza A virus-exposed epithelial cells

The human lung epithelial cell line A549 used was cultivated in DMEM (PAA) supplemented with 10 % heat-inactivated fetal bovine serum (FBS, Biochrom). Conventional object slides were used. One day prior to infection, cells were seeded on cover slides at 80 % of confluency. For influenza A virus (IAV) infection, the cells were inoculated with influenza virus A/Puerto Rico/8/34 (H1N1). To allow the IAV particles to attach, the cells were incubated at 4 °C for 1 h after addition of the inoculum. Cells were fixed with formaldehyde for further processing.

For SPDM, two different treatments were applied:

Antibody labeling of IAV coat proteins

Immunofluorescence labeling of IAV coat proteins with Alexa488 as reporter fluorophores and incubation with A549 cells was performed according to standard protocols.

Antibody labeling of a potential IAV receptor protein complex

Cells were treated with recombinant human growth factor/HGF (R&D Systems) at a concentration of 30 ng/ml (in Opti-MEM). The inoculum of the negative controls just contained medium (Opti-MEM + Glutamax, Invitrogen); the positive controls contained medium and HGF (final concentration 30 ng/ml) and the inoculum of IAV treated cells contained medium and virus particles at a multiplicity of infection (MOI) of 100 (this means on average 100 infectious particles per cell). Thereafter, all cells treated in this way were incubated at 37 °C in a standard CO_2 incubator for the times indicated (5, 10, 15 and 30 min) before they were fixed on the cover slip and labeled. For this, the inoculum was removed; cells were washed twice with PBS and fixed with formaldehyde (Roth, 3.7 % v/v in PBS) at room temperature (RT) for 20 min. For permeabilization, cells were then incubated with 0.2 % (v/v) Triton X 100 at RT for 2 min. Immunofluorescence labeling was performed using rabbit anti-HGFR polyclonal antibodies and Alexa488-labeled goat anti-rabbit antibodies. For further details, see (Wang et al. 2014).

Expression of viral proteins

For generation of vector pEYFP-m164 expressing the glycoprotein gp36.5/m164 from murine cytomegalovirus fused to EYFP (enhanced yellow fluorescent protein), the corresponding viral gene was amplified by PCR, using primer pair m164_EcoRI_for (5′-CGTGGAATTCTCGCCGCCATGTTTCTCCGCGGC-3′) and m164_BamHI_rev (5′-AAGGGATCCTCTGACGAACGTCCGACGC-3′). Purified viral DNA derived from the mCMV-Wildtype strain Smith (ATCC VR-194/1981, re-accessioned as VR-1399) served as the template. The corresponding fragment was cloned via the EcoRI/BamHI restriction sites into the pEYFP-N1-vector backbone.

COS-7 cells were grown on glass cover slips for 24 h. Expression vector pEYFP-m164 was transiently transfected into the COS-7 cells by using PolyFect transfection reagent. Cells were fixed 48 h post-transfection with 4 % (w/v) formaldehyde freshly prepared from paraformaldehyde, and the cover slips were mounted in ProLong Gold antifade reagent (catalog no. P36930, Life Technologies) for storage at 4 °C in the dark. For more details, see (Müller et al. 2014).

Results

Localization microscopy/SPDM of virus particle morphology and aggregation state

To elucidate the potential of localization microscopy/SPDM to study morphology, functionalization and aggregation status of virus particles, tobacco mosaic virus (TMV) was employed due to its high potential and increasing use as multivalent elongated bioscaffold in functional materials (e.g., Wu et al. 2010; Atanasova et al. 2011; Eber et al. 2013), miniaturized devices (Alonso et al. 2013) and medical imaging (e.g., Bruckman et al. 2013).

Tobacco mosaic virus is a robust, self-assembling tube-shaped plant virus of 300-nm natural length and 18 nm diameter, with an inner longitudinal channel 4 nm in width. Its protein shell consists of 2,130 identical, helically arranged coat protein (CP) monomers, interacting with a single buried RNA molecule determining the final length of the viral particle. By biochemical and genetic engineering techniques, different TMV-derived nanotube biotemplates of pre-determined aspect ratio and with tailored surfaces have been produced (Kadri et al. 2011; Geiger et al. 2013; Eiben et al. 2014). For the SPDM measurements reported here, a TMV mutant (T158K with a natural CP threonine moiety exchanged for a lysine, hence named TMV_{Lys}; Geiger et al. 2013) presenting an amine functionality on every CP subunit on its outer surface was used, which was exploited for covalent fluorescent labeling of the viral particles at non-disruptive conditions.

Figure 1 highlights the capability of localization microscopy/SPDM to identify the shape of a virus particle, in contrast to the conventional widefield image. While in the latter case it was impossible to visualize the plant viruses as rodlike thin structures, the localization microscopy/SPDM image allowed the clear identification of these nanostructural elements. A detailed quantitative analysis (Gunkel 2011) revealed a length of these particles typically around 300 nm (or multiples). Furthermore, fluorophore density profiles across the virus structures were extracted, showing typically a Full-Width-at-Half-Maximum (FWHM) around 60 nm. For extraction of the virus diameter, these profiles were deconvolved (using a least square fit) with the effective lateral PSF of the localization microscopy, as generated from the values for the localization accuracy. A detailed comparison of the individual molecule positions in several hundred TMVs with numerical models of cylindrically shaped TMVs (Gunkel 2011) indicated a diameter (FWHM) of ca. 20 nm, i.e., values very close to those obtained from EM and crystallographic data.

The high structural resolution of virus particles by SPDM as visualized in Fig. 1 may be used to determine the overall distribution pattern of functional molecules on the viral scaffold, a beneficial analytical tool for future applications of non-evenly functionalized biotemplates (Geiger et al. 2013), and to ascertain the aggregation state of such objects in a larger region of interest (ROI) directly after deposition to the slide from an aqueous suspension and hence to count reliably the number of monomeric as well as laterally or head-to-tail aggregated virus particles in this ROI. From this, an estimate on the homogeneity of nanoparticle suspension and corresponding local virus densities may be obtained.

Figure 2 shows an example for the 'nanoimaging' of the aggregation and counting of virus particles by localization microscopy/SPDM. While in the example shown in Fig. 2a, the conventional resolution image still allows a first rough estimate of the virus distribution and concomitant particle aggregation state, a more exact quantitation cannot be achieved. This, however, became possible by application of the SPDM mode: Each virus particle in the ROI shown in Fig. 2b is clearly identified by its rodlike shape. On the basis of morphology, 102 TMV particles were manually counted in a region of interest of 62 μm^2, resulting in an estimated virus density of $\rho_{virus} = 1.6 \times 106/mm^2$ with several laterally or head-to-tail aggregated nanotubes. This confirms numerous earlier observations on an extensive aggregate formation and 'multimerization' of TMV particles, which depends on the nanorods' physicochemical environment, but is difficult to determine in a quantitative manner by ultra-resolution imaging techniques: Sample preparation for electron or atomic force microscopy may promote deposition artifacts and thus affect the TMV aggregation status if, e.g., buffer exchanges, mechanical spreading or airstream drying methods, substrate surface coatings or chemical fixatives are employed. By contrast, localization microscopy can use a broad range of TMV nanorod formulations in different solvents or buffers, from which the viral particles are immobilized gently and slowly to non-treated or, e.g., silane-modified slides, with optional washing steps removing salt and other contaminants after TMV settling. In combination with the large substrate areas analyzable by SPDM thereafter, the average percentage of laterally or head-to-tail aggregated nanoparticle dimers and oligomers may be determined exactly and easily for a certain TMV preparation, with the need of only a low number of specimens to ensure statistically firm data.

Nanoimaging of virus-cell association

A decisive stage in the infection cycle of animal viruses is the interaction of virus particles with the cell membrane, as the first step prior to cell penetration and uncoating. As an example for the potential of localization microscopy to elucidate such entry mechanisms, we here report on the use of SPDM to highlight the close spatial association of influenza A viruses to human lung epithelial cells.

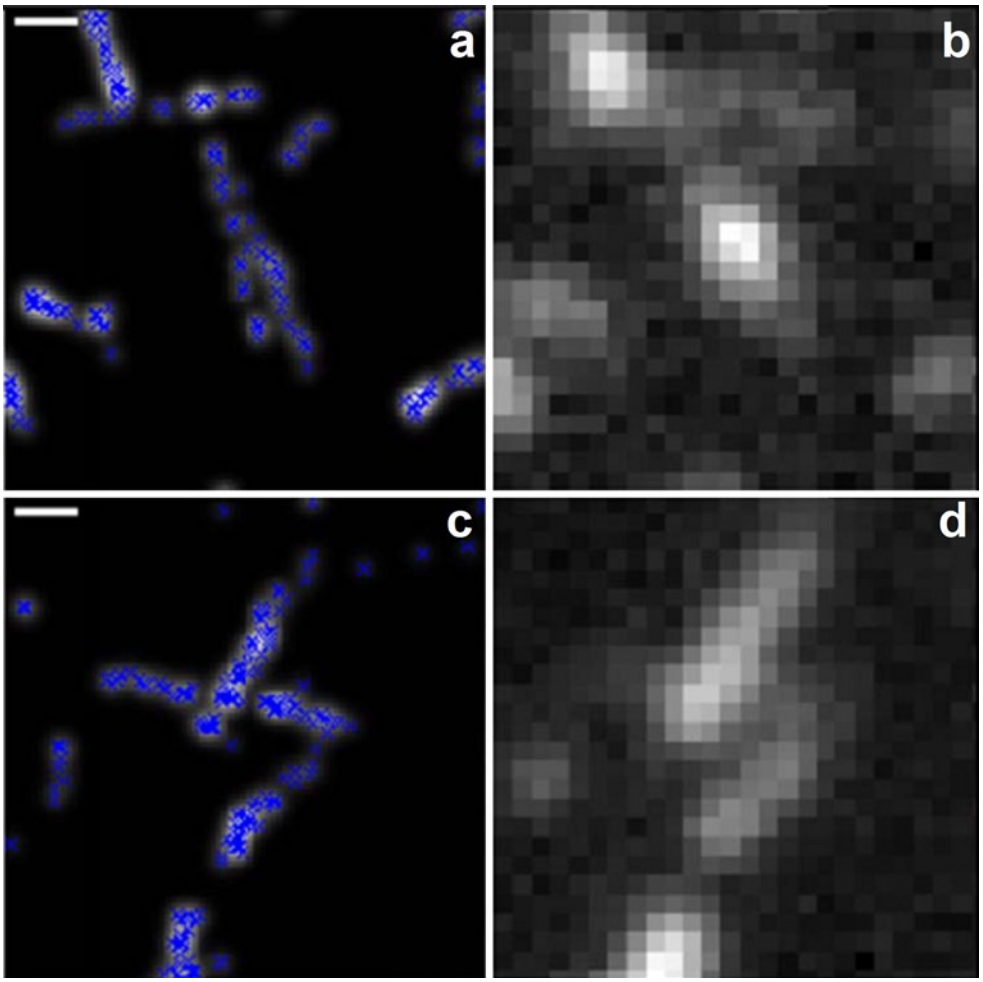

Fig. 1 Localization microscopy/SPDM of virus morphology. SPDM images of TMV particles with coat proteins (CPs) labeled with the fluorophore Atto488. **a**, **c** In the two SPDM images from two different regions of interest, the individual dye molecule positions are blurred by a Gaussian function with a standard deviation corresponding to the individual localization accuracies; the molecule positions determined are indicated by *blue crosses*. **b**, **d** Corresponding conventional microscopy images taken with the same microscope optics (NA = 1.4) and excitation wavelength (λ_{exc} = 488 nm). *Scale bars* (**a**, **c**) valid also for images in **b**, **d** are 200 nm. From Gunkel (2011)

Influenza A virus (IAV) is capable of rapid genetic changes in mammals. It is an important pathogen that causes acute diseases of the respiratory tract in millions of people each year all over the world. The IAV subtype H1N1 is currently endemic in both human and pig populations (Spicuzza et al. 2007; Swayne and Halvorson 2008).

Figure 3 shows an example for the SPDM analysis of the close apparent association of IAV particles to the membrane of human lung cells. In this case, an IAV coat protein was immunostained using fluorescence-labeled antibodies. While it was impossible to reveal any peculiarities of the virus association in the conventional resolution wide-field image (Fig. 3a), this was clearly indicated in the SPDM image (Fig. 3b). This image indicates the result of an analysis where all molecule positions assigned to clusters containing at least 10 signals were presented in the SPDM image, blurred with the localization accuracy.

The diameter of these IAV protein clusters was found be on average about 120 nm, i.e., close to the size of IAV virus particles determined by electron microscopy. Hence, the SPDM image indicates the possibility to count the individual IAV protein clusters along the membrane, in contrast to the conventional resolution image. Since only the virus particles had been labeled in these 'one color' SPDM experiments, it was not possible to measure the exact distance to the cell membrane. However, together with dual color SPDM of a cell membrane protein, it should become possible to determine even the attachment sites to the cell membrane with accuracies in the range of a few nanometers.

SPDM analysis of virus-receptor interactions

The interaction of virus particles with cell membrane receptors is one of the most critical steps in infection. As

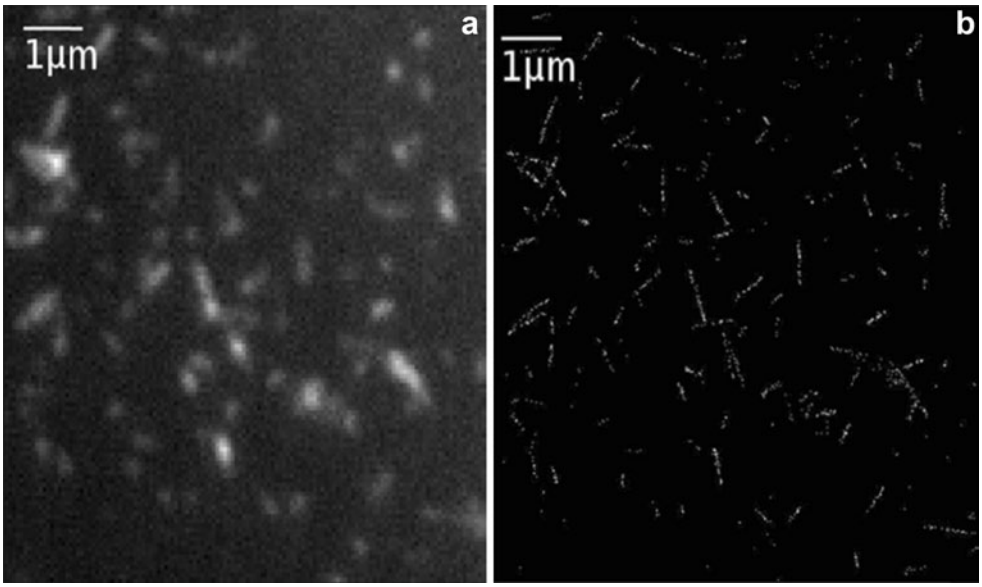

Fig. 2 Localization microscopy/SPDM of virus aggregations. **a** An area covered with Atto488 fluorescently labeled TMV particles of different aggregation at conventional optical resolution. **b** The same region of interest visualized in the SPDM mode. Individual TMV viruses are visible as small rodlike structures, in several cases laterally or head-to-tail adjacent to each other. The *small dots* along these *rodlike structures* denote the position of individual Atto488 dye molecules coupled to coat proteins. *Scale bar* 1 µm. For further details, see Fig. 1 and text. From Gunkel (2011)

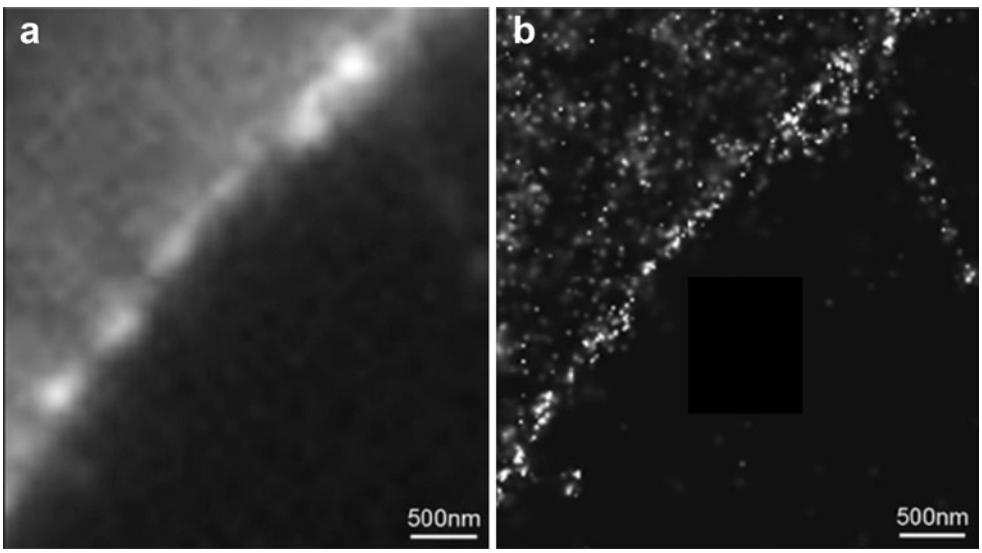

Fig. 3 Localization microscopy/SPDM of human influenza A virus association to a cell membrane. **a** Conventional fluorescence microscopy of Alexa488 immunostained IAV viruses associated to A549 cells. Shown is only a part of the cell ($\lambda_{exc} = 488$ nm). **b** SPDM nanoimage of the same cellular region as in **a**. The positions of the individual fluorescent antibody molecule signals detected ($\lambda_{exc} = 488$ nm) within clusters containing at least 10 signals were Gaussian blurred with the localization accuracy σloc of the individual fluorescent signals. *Scale bars* 500 nm (original data)

a methodological example, here, we show the application of localization microscopy/SPDM to study a possible influence of IAV infection on the spatial distribution of a specific membrane receptor complex in human cells.

Previous studies (Eierhoff et al. 2010) have presented first indications of an interplay of IAV with receptor tyrosine kinases (RTKs). If so, RTKs would be expected to play a role in the mechanism of IAV entry into the cells. It is

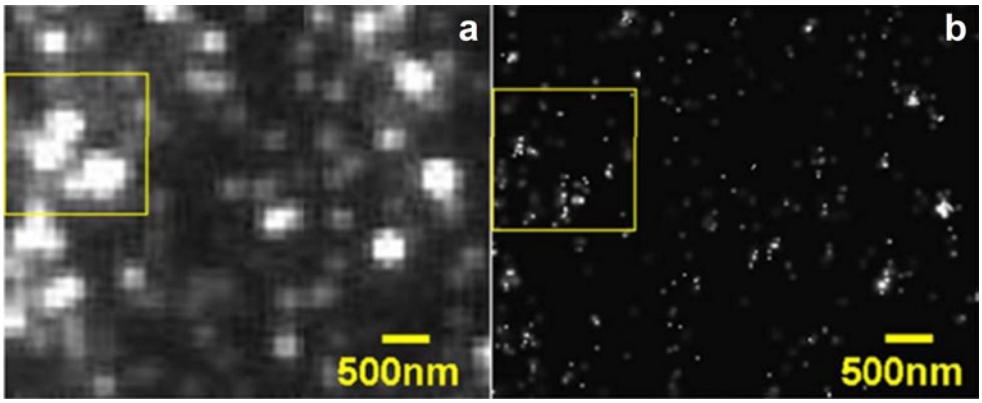

Fig. 4 Localization microscopy/SPDM of Alexa488 immunostained HGFR protein clusters on the membrane of A549 cells. **a** Wide-field fluorescence microscopy (conventional resolution) of a small part of an A 549 cell membrane. **b** SPDM image of the same cellular region as shown in **a**. The SPDM image was obtained after blurring of the individual HGFR localization maps with a Gaussian corresponding to the localization accuracy of the individual fluorescent signal (the mean localization accuracy of all signals was σloc = 29 nm). As an example, the inserts highlight specifically the enhancement of resolution by SPDM. While in the conventional resolution insert (**a**), three large clusters of several hundred nm in diameter are observed, in the SPDM resolution insert (**b**), these are resolved in multiple clusters, each of them substantially smaller than 100 nm. *Scale bars* 500 nm. From Wang et al. (2014), modified

hence of great importance to study the effects of IAV on specific RTK receptor molecules on the cell membrane and the influence on their spatial distribution. In this report, we discuss the use of localization microscopy/SPDM to study on the single-cell/single-molecule level a possible relationship between IAV infection and changes in the spatial distribution of the membrane based Hepatocyte Growth Factor Receptor (HGFR) in human alveolar basal epithelial cells. HGFR (Bottaro et al. 1991; Galland et al. 1992) is a protein encoded by *c-met* that is a proto-oncogene related to process tyrosine kinase activity (Cooper 1992). The HGF receptor (HGFR) is a major regulator of proliferation, migration. Via its binding, HGFR transduces multiple biological effects such as mitogenesis, motogenesis, metastogenesis and morphogenesis (Bottaro et al. 1991; Weidner et al. 1993; Zwick et al. 2001).

Figure 4 shows a conventional wide-field image (a) and a localization microscopy/SPDM image (b) of a small part of an IAV virus-infected cell after an incubation time of 5 min. Already from the conventional resolution image (a), it is obvious that the spatial distribution of the HGFR proteins on the cell membrane is highly heterogeneous; obviously, many of them are arranged in small clusters. The conventional resolution image (a) suggests that these clusters might even be as large as several hundred nm in diameter, corresponding to the optical resolution limit. Using localization microscopy (SPDM, b), the visual inspection confirms the highly heterogeneous distribution of the HGFR clusters already visible in the conventional resolution images. The SPDM images indicate, however, that first, the number of clusters is much larger than detected in the conventional resolution images and second, the size of the clusters is in reality much smaller (below 100 nm). A detailed quantitative analysis (Wang et al. 2014) of about 44,000 of such clusters revealed a mean cluster size of 54 ± 24 nm.

In this previous report (Wang et al. 2014), we studied the number of HGFR molecule signals present within and outside clusters as a function of the treatment (after IAV infection; with HGF ligand only; without IAV and without HGF) and various incubation times. It turned out that on the average, around 20–25 % of all HGFR signals were found to reside in clusters of about 50 nm diameter. Surprisingly, in contrast to the considerable variations of the absolute numbers of HGFR proteins detected in the individual experiments, the HGFR protein densities (obtained by an automatic algorithm) in the clusters turned out to be quite stable: The overall variation in the density values for different treatments and incubation times was around 10 % only; in the individual groups, the standard deviation in the protein density was around 5–7 %.

Using the average diameter obtained from the density related algorithm for the HGFR clusters (54 nm), a first estimate was obtained for the number of HGFR molecule signals detected in an individual cluster (Wang et al. 2014). Altogether, the number of HGFR molecule signals per cluster (N_{CL}) obtained with this estimate was between 5 and 6. These first estimates, however, did not consider the variation in diameter (standard deviation ± 24 nm): Since the cluster defining circular area is proportional to the square of the diameter, the number of HGFR molecule signals/cluster determined from multiplying the density with the cluster area becomes highly sensitive to changes in the diameter. A change of ± 24 nm in the diameter $d_{cluster}$ corresponds

to a 2–3 times change in the cluster area $A_{cluster}$ compared with the average area, and a similar change in the estimated N_{CL} values. Here, we report an improved way of estimate which does not require knowledge of the cluster diameter but only of the total cluster number and of the total number of HGFR molecule signals within the cluster.

To obtain this second estimate for NCL, for each condition, the total number of several thousand HGFR molecules N_{tot} detected in the clusters was counted on the basis of the individual molecule positions by an automated image analysis procedure. This number was combined with the total number of clusters $n_{cluster}$ obtained under a special condition. The values for $n_{cluster}$ were also identified by an automated procedure (Wang et al. 2014). To obtain by this method an estimate for the number N_{CL} of HGFR molecule signals/cluster, for each treatment and incubation time, N_{tot} was divided by $n_{cluster}$: $N_{CL} = N_{tot}/n_{cluster}$. The result is shown in Table 1.

As a result, for the mean number N_{Cl} of HGFR signals per individual cluster in all the 240 cells measured under 12 different conditions, containing a total of 44,304 clusters with a total of 231,659 molecule signals in these clusters, the value $N_{CL} = 5.2 \pm 0.5$ HGFR molecule signals/cluster was obtained. This second estimate is very similar to the first estimate obtained from the protein densities and the average cluster size (5–6 HGFR molecule signals per cluster); however, since in the second estimate, only the cluster number $n_{cluster}$ and the molecule signal numbers N_{tot} in the clusters were used and not the cluster size $d_{cluster}$, the value $N_{Cl} = 5.2 \pm 0.5$ HGFR molecule signals/cluster may be regarded more reliable; on the other side, the surprisingly good coincidence between the two different ways to estimate the number of HGFR signals/cluster suggests that the value derived for the average cluster size (54 nm Ø) is reliable.

SPDM of viral protein expression

The importance of CD8 T-cells for the control of cytomegalovirus (CMV) infection has raised interest in the identification of immunogenic viral proteins as candidates for immunotherapy. The 36.5 kDa gene product of the murine cytomegalovirus (mCMV) ORF *m164* (Holtappels et al. 2002a, b) is indicative of such a protein. Protein gp36.5/m164 has been identified as an integral type-I membrane glycoprotein with exceptional intercellular trafficking dynamics, moving along the outer nuclear membrane and within the endoplasmic reticulum (ER) with high lateral membrane motility (Däubner et al. 2010). Vector pEYFP-m164, encoding the mCMV glycoprotein gp36.5/m164 fused to eYFP (enhanced yellow fluorescent protein), was transiently transfected into COS-7 cells. After transfection, the accumulations of gp36.5/m164 were represented by SPDM on the nanoscale and displayed different protein density distributions in the diverse structural cytoplasmic and membrane associated regions (Müller et al. 2014). In contrast to wide-field images, the SPDM images allow a single-molecule resolution of the protein assembly that can contribute to the identification of immunogenic viral proteins as candidates for vaccination and cytoimmunotherapy.

Figure 5 gives an example for the SPDM 'nanoimaging' of the expression of the eYFP-tagged viral glycoprotein gp36.5/m164 in COS-7 cells. While the conventional wide-field fluorescence image indicates a heterogeneous distribution of the expressed proteins in the cytoplasm, due to an insufficient resolution it prevents any more detailed analysis; as the inserts demonstrate, it precludes any possibility to resolve the proteins individually. The SPDM image of the same cell, however, shows a substantially enhanced resolution and demonstrates different arrangements of the gp36.5/m164 proteins. The magnification of the inserts in the SPDM image (at the same sites as the inserts in the wide-field image) shows this in more detail. To better highlight the differently shaped arrangements and to provide an idea for the optical (two-point) resolution obtained, in this SPDM image the individual molecule signals were blurred with the localization accuracy. For a detailed quantitative evaluation of the single-molecule positions and structural interpretation measured with the SPDM method, see (Müller et al. 2014).

Table 1 Mean number NCl of HGFR signals per individual cluster

	Control	Ligand (HGF)	Virus infection
5 min	18,865/3,683 = 5.1	14,254/2,902 = 4.9	26,697/4,417 = 6.0
10 min	21,539/4,181 = 5.2	22,787/4,237 = 5.4	22,788/4,448 = 5.1
15 min	14,494/2,975 = 4.9	20,262/3,941 = 5.1	19,751/3,841 = 5.1
10 min	9,364/2,119 = 4.4	16,440/3,644 = 4.5	24,417/3,916 = 6.2

N_{CL} = (Total number N_{tot} of HGFR signals detected in the cluster detected for a specific treatment)/(total number $n_{cluster}$ of cluster detected for a specific treatment) (total no. of cells: 240, each condition 20 cells). Original data

Discussion

Since its introduction in the 1990s, superresolution light microscopy ('nanoscopy') of biostructures has found an ever broadening field of applications in cell biology. The respective methods offer, however, also highly interesting opportunities in virology, for understanding mechanistic details of virus-host interactions as well as for exploiting virus-derived nanoparticles in novel technologies and devices. Here, we concentrate on some aspects made possible by the introduction of localization microscopy techniques. In this discussion, we focus on perspectives in both

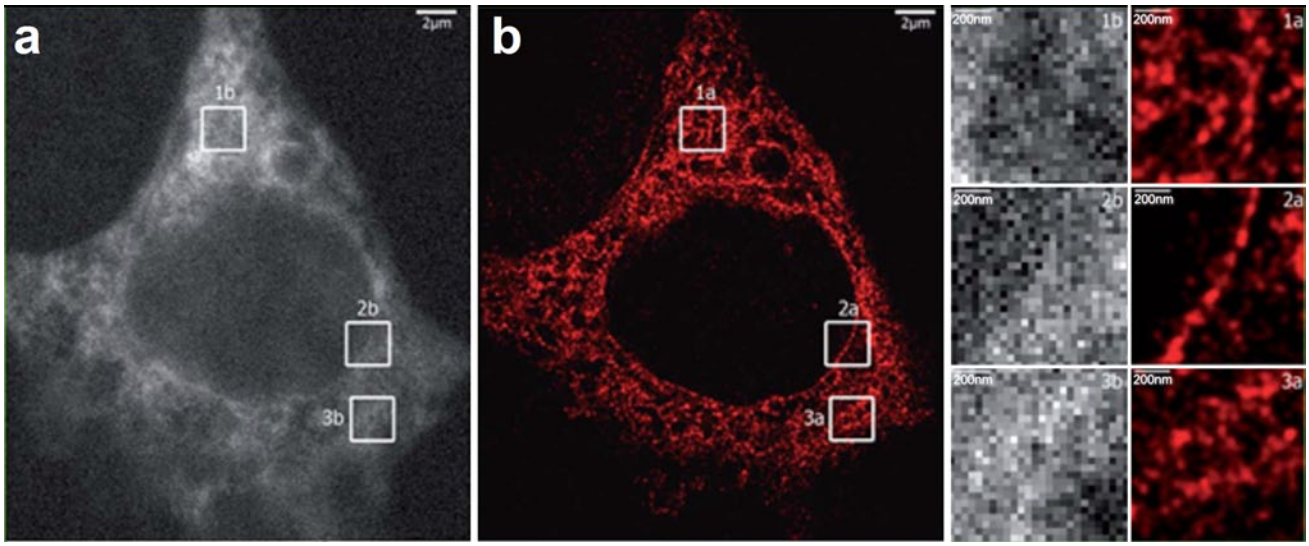

Fig. 5 Expression of viral proteins by localization microscopy: SPDM images of eYFP-tagged gp36.5/m164 proteins in COS-7 cells. **a** Conventional wide-field fluorescence image (EPI); **b** SPDM image; *Insets* Magnification of three sections of the wide-field image (1b, 2b, 3b) and of the identical sections in the SPDM image (*1a*, *2a*, *3a*). In the SPDM image and inserts, the individual fluorescent signals were blurred with the individual localization accuracy. From Cremer et al. (2011)

molecular virology and virus-deduced tools as suggested by our present experience in SPDM; we anticipate, however, that similar applications will be possible also by other localization microscopy techniques.

Perspective 1: 'Nanoimaging' of virus-cell membrane interaction

Recently, localization microscopy methods have been used in virological research to study the attachment of HIV particles to the cell membrane (Muranyi et al. 2013). For this, a dSTORM (direct stochastic optical reconstruction microscopy) technique was applied (Heilemann et al. 2008), which is related but not identical to the SPDM-based localization microscopy approach described in this report (for further discussion, see Cremer and Masters 2013). The experimental results reported here indicate that SPDM is also a suitable technique to study the attachment of viruses to the cell membrane. In contrast to the HIV studies mentioned, we concentrated on the influenza virus (IAV), another virus of global health importance. The results indicate that it is possible to identify and hence count the IAV particles along the cell membrane. With an appropriate localization accuracy, also functionally induced heterogeneities in the spatial distribution of the IAV coat proteins will be accessible to quantitative measurements. Using dual color SPDM (Gunkel et al. 2009; Cremer et al. 2011), it should be possible to distinguish between virus and membrane proteins, and thus be able to measure virus-membrane distances with an accuracy of few nanometer. It may be noted that in this case, relevant information on virus-membrane interaction would already be obtained by a 'two color' SPDM technique where only the distance between the bary center (fluorescence intensity centroid) of the protein coat ('color' A) of an individual virus and an individual membrane receptor protein ('color' B) is measured: For example, in the case of a spherical virus with a diameter of 120 nm, such a 'two color' SPDM distance would be expected to be in the range of 60–70 nm. Such measurements would require a two-point resolution and hence a localization accuracy in the range of few tens of nm (i.e., two signals A, B detected within an area of ~200 nm would already be sufficient) but not a high structural resolution (i.e., multiple molecule positions discriminated within an area of ~200 nm). Such 'two color' SPDM measurements can be performed also with photostable fluorophores, i.e., they do not require photoswitching (Esa et al. 2000, 2001; Rauch et al. 2008). This highly facilitates the possibility to perform such studies even in the living cell. Compared with FRET measurements (Fluorescence Resonance Energy Transfer) with a maximal interaction distance of 10 nm, the 'two color' SPDM measurements would allow to measure also larger distances between virus and membrane.

Localization microscopy may also be used to obtain an improved mechanistic view of the details of interactions between virus particles attached to the membrane and specific receptor protein clusters on or within the membrane. To highlight this possibility, as an example, we investigated by SPDM the spatial distribution of HGFR proteins on the membrane of IAV-infected human lung cells. Previous

findings (Wang et al. 2014) had already indicated that the size of the HGFR clusters was not affected by the virus infection to a larger degree: In both IAV-infected and non-infected cells, the diameter of the HGFR clusters was about 50 nm; since this was close to the size resolution limit of these SPDM measurements, it is still possible that an enhanced resolution will reveal differences. In any case, if such differences in cluster size between infected and non-infected cells exist, they are expected to be smaller than a few tens of nanometer.

In this report, additional data were presented on the relative number of individual HGFR molecules counted in these clusters. This was done by dividing the total number of molecule signals within the clusters by the total number of clusters detected for a given treatment. In this way, any dependence on the cluster size itself as used in the previous estimate by Wang et al. (2014) was eliminated. The results confirmed in a direct way that the number of molecules in the HGFR clusters is very similar in both IAV-infected and non-infected cells, suggesting the formation of specific complexes.

Perspective 2: Expression of viral genes

To replicate, after infection of the host cell, viruses have to uncoat and express proteins; in addition, viruses might be used in gene therapy once appropriate vectors can be found. In both cases, it is highly desirable to determine quantitatively the expression and intracellular distribution of specific virus-encoded proteins on the single-cell level. To indicate the suitability of SPDM to perform such expression studies, in this report, SPDM images of cells have been presented with the expression of virus eYFP-tagged glycoprotein gp36.5/m164. While conventional wide-field microscopy was not suitable to resolve the virus-encoded glycoproteins expressed, SPDM revealed their spatial distribution inside the cell on the molecular scale. A more detailed quantitative analysis of the SPDM expression data is given in an accompanying paper (Müller et al. 2014). It is anticipated that localization microscopy will become a valuable technique to complement bulk measurements of virus-encoded protein expression on the level of individual molecules in specific intracellular regions (e.g., membrane, endoplasmic reticulum, nucleus) of individual cells at unprecedented resolution. This will allow us to obtain a more detailed idea of the heterogeneity of virus-encoded expression, e.g., in individual cells in a tissue section.

Perspective 3: Optimization of (plant-) virus-based nanotools and biodetection devices

While derivatives of mammalian viruses are currently being developed into vectors, e.g., for gene delivery or vaccination, bacteriophages and especially robust plant viruses contribute rapidly emerging building blocks to novel biohybrid nanodevices and functional ‘smart’ materials. Both native as well as modified plant viruses and virus-like particles are multivalent nanoscaffolds, exposing a multitude of precisely ordered functional groups on outer and/or inner protein surfaces. Various particle shapes are available, ranging from spherical nanocontainers to flexible or stiff filaments or tubes, respectively, which can be harvested in high amounts from plants and, in some cases, from heterologous expression systems. Numerous applications as high surface area nanobiotemplates, e.g., for the directed deposition of functional inorganic and organic compounds seem realistic, e. g., in energy-converting, electronic and optical devices (for an overview, see, e.g., Alonso et al. 2013; Lee et al. 2012; Steinmetz and Manchester 2011).

Since plant virus-based nanoscaffolds are non-pathogenic for any warm-blooded animal, the use of non-denaturated virus-derived structures for the high density presentation of complex functions such as antibodies, enzymes and effector proteins is attracting increasing attention as well, since it offers novel routes toward the directed integration of biofunctionalities into miniaturized biodetection and even catalytic devices. Furthermore, it allows the combination of different functions on and in single nanosized carriers, which is extensively analyzed to achieve targeted biocompatible imaging and concomitant drug delivery, e.g., to tumor tissues or thrombotic veins (for a recent overview, refer, e.g., to Bittner et al. 2013). Several applications demanding for concerted protein actions or the combinatorial presence of diverse active units can profit from an ordered presentation of the respective functions on the nanoscale, i.e., from an installation of cooperating proteins and putatively additional molecules on pre-determined domains of viral backbones (Cardinale et al. 2012; Geiger et al. 2013).

For all these approaches making use of selectively addressable sites on viral protein shells, outside or inside technical devices or mammalian cells, ‘nanoscopy’ may serve as a powerful novel tool allowing an unprecedentedly efficient characterization of the composite virus-scaffolded effector architectures. Currently, high-resolution analyses of viral hybrid nanoparticle preparations frequently suffer from preparation conditions if electron microscopical methods are applied, abolishing functionality of reporter, catalytic or recognition elements exposed on viral templates. The ambient conditions compatible with SPDM and related techniques are a major advantage in this context, and thus may lead to high-resolution studies not only of the patterns of virus template-immobilized active molecules, but even on their putative collaborative activities if resulting in the formation of fluorescent products in situ. Different from near-field techniques such as apertureless scanning near-field optical microscopy (aSNOM) recently established

successfully for high-resolution topography analyses of fluorescently labeled TMV (Harder et al. 2013), the wide-field mode of operation adds special advantages: It may provide a reliable representative overview of large amounts of nanoparticles within applicable formulations, with respect to their homogeneity and aggregation state, as demonstrated above. Finally, if applied to a technical substrate equipped with virus-exposed functional units at pre-selected sites (Blum et al. 2011; Mueller et al. 2011; Azucena et al. 2012), SPDM and other 'nanoscopy' variants can provide both functional and positional information on extended areas simultaneously, which may speed up the development of advanced biohybrid chips employing viral adapter templates for complex functionalities, e.g., in the ultrasensitive detection of hormones or toxic compounds in medicine, environmental monitoring or foodstuff inspection.

Perspective 4: Identification of viruses by oligonucleotide labeling

Every year, hundreds of millions of women and men are infected by various types of viruses; several millions of them die each year by such infections; hence, it is important to develop fast methods to identify specific virus types, not only within cells but also in the environment, including public buildings, schools, hospitals. Important virus types to be monitored include a variety of influenza and oncogenic viruses. For example, it should be highly useful to develop more sensitive tests for human papilloma viruses. Another example would be the improved control of food for the presence of noroviruses. Although PCR (polymerase chain reaction) techniques offer efficient ways to detect the presence of specific types of viruses, it is still difficult to map with a high spatial resolution in an economical, direct and highly quantitative way the presence and aggregation state of certain viruses in specific cells (e.g., in cancer tissue), or in environmental 'hot spots'. As an example, the SPDM images of TMV and IAV particles presented in this report indicate that—provided appropriate fluorescence labeling—such viruses and their aggregation status can be ascertained directly by localization microscopy. In principle, localization microscopy should allow us to detect an individual virus particle in a single cell.

In the SPDM images of viruses shown, coat proteins were fluorescently labeled, either by using antibodies, or by direct labeling using a click chemistry technique. In the following, we describe the concept of an additional way of fluorescence labeling, which will allow us to identify by localization microscopy/SPDM a large number of viral particles of the same shape but with differences in their genome sequences.

For clarification of the concept, let us assume that a variety of closely adjacent virus particles of similar shape (e.g., spherical, around 50–100 nm diameter) but with differences in their genome sequence has to be identified. For simplicity of argument, we assume that all these genomes have a single-stranded RNA/DNA with a length of about 10–15 kb. Medically important viruses of this class are, e.g., HIV, HPV, Influenza A, or Hepatitis C viruses. Various strains of these viruses might be present; hence, in the end, multiple viral genomes have to be identified on the single virus level at a given location, and the number of each type and its aggregation state has to be determined. For this, it should be possible to use SPDM (or another suitable localization microscopy technique) after labeling with combinatorial oligonucleotide fluorescence in situ hybridization (COMBO-FISH) (Grossmann et al. 2010; Hausmann et al. 2003) or related methods like oligonucleotide painting (Beliveau et al. 2012) to distinguish the various virus particles from each other. For example, N types of virus particles with differences in their sequence have to be distinguished by COMBO-FISH and SPDM from each other. In this labeling scheme, combinations of n different reporter molecule types have to be identified which can be distinguished by their fluorescence behavior.

Generally, with n reporter molecule types, $N = 2n - 1$ different viral sequences should be distinguishable by combinatorial labeling, in a way analogous to combinatorial chromosome painting (Cremer and Cremer 2001; Bolzer et al. 2005). While stochastic blinking by itself is a very useful tool to localize single molecules, additional differences in the 'spectral signature' are required to further identify the blinking molecule types independently from each other. For this, differences in the absorption/emission spectrum or in the fluorescence life time may be used (for simplicity called 'color' in the following). In many cases, it should even be sufficient to perform the localization microscopy/SPDM-based identification using combinations of photostable reporter molecule types alone (Cremer et al. 1999; Esa et al. 2000, 2001; Rauch et al. 2000, 2008; Heilemann et al. 2002). This latter approach should allow the use of sufficiently low illumination intensities to make possible also in vivo studies. As an example for SPDM-based virus identification, 7 different virus types have to be distinguished by COMBO-FISH. For this, let us assume that virus type #1 contains a sequence difference s1 (e.g., with a total labeled length hundred nucleotides); virus type #2 contains another sequence difference s2 of similar length, etc. Then, e.g., a set S1 of three oligonucleotide sequences of 30 nucleotides (nt) each tagged with 'color' A is synthesized to be complementary to sequence s1; a second set S2 of three oligonucleotide sequences of 30 nt each (different from s1) tagged with 'color' B is synthesized to be complementary to sequence s2; a third set S3 of three oligonucleotide sequences of 30 nt each tagged with 'color' C is synthesized to be complementary to sequence

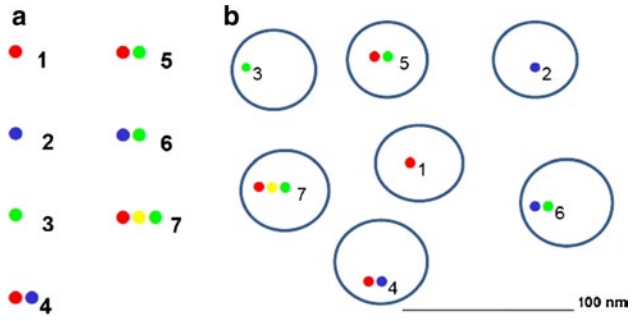

Fig. 6 Combinatorial oligonucleotide FISH (COMBO-FISH) labeling scheme for identification of viral sequences by localization microscopy/SPDM. **a** Schematic combinatorial labeling scheme of viral sequences assuming $n = 3$ 'colors', e.g., 3 differences in the absorption/emission spectrum, or the same absorption/emission spectrum and 3 distinguishable fluorescence lifetimes; the SPDM imaging may be performed either in the photoswitching mode, or with photostable reporter molecules. **b** In a region of interest with close aggregations of different virus particles (assumed size here ~ 50 nm), these can be identified independently from each other by the combinatorial labeling as long as the SPDM positions observed for the same 'color' have a distance larger than the viral diameter (indicated schematically by *blue circles* around the COMBO-FISH signals). *Scale bar* 100 nm

s3 (different from s1 and s2); a set S4 contains three oligonucleotide sequences (different from s1–s3), one labeled with 'color' A and one labeled with color B, etc. A mixture of the synthesized, fluorescent-labeled oligonucleotides is then hybridized to the virus specimen, and localization microscopy/SPDM is performed.

Figure 6 shows a graphical representation of this combinatorial approach for $n = 3$ 'colors'. With $n = 7$ 'colors', it would be possible to identify $27–1 = 127$ different types of viruses; with $n = 10$ 'colors' (Dempsey et al. 2011; Herzenberg et al. 2002), already $210–1 = 1{,}023$ different virus types would be distinguishable by localization microscopy/SPDM and COMBO-FISH.

In the example indicated in Fig. 6 for $n = 3$ 'colors', it was assumed that the distance between the viruses is too small to allow the identification of the individual particles by conventional fluorescence microscopy (optical resolution ~200 nm). In case of low virus density (i.e., the distances are sufficiently large), also standard fluorescence microscopy might be used. However, in cases where a low virus density cannot be predicted safely, localization microscopy/SPDM-based approaches are expected to be more reliable. In addition, the use of COMBO-FISH-based localization microscopy/SPDM might be most advantageous even in the case of low virus density, if the viruses have to be identified within cellular structures: In this case, due to cellular background fluorescence, the limits of detection sensitivity of DNA/RNA sequences are typically in the range of several hundred bp to several kpb for one 'color'. Thus, due to the relatively small total sequence length of many virus types, it will be difficult to obtain sufficient signal strength for the required 'multi-color' labeling (e.g. $n = 7$).

It may be noted that instead of using a combinatorial labeling scheme for DNA/RNA, a similar combinatorial labeling scheme might also be applied for the coat proteins (Cremer et al. 2003). For example, if a virus type 1 is characterized by a coat protein 1, a virus type 2 by a coat protein 2, a virus type 3 by a coat protein 3, etc., for identification of the viruses, one might use a mixture containing antibodies 1 against protein 1 (virus 1) tagged with 'color' A; antibodies 2 against protein 2 (virus 2) tagged with color 2; the antibodies against protein 3 might consist of a mixture of antibodies 3 with 50 % tagged with color A and 50 % tagged with color B. As a consequence, viruses 1 are labeled A, viruses 2 are labeled B; viruses 3 are labeled A/B; for multicolor labeling, the same combinatorial rules apply like those described above for DNA/RNA sequences. The advantages of localization microscopy/SPDM for virus identification by combinatorial coat labeling are also analogous to those discussed above.

To summarize, localization microscopy methods are expected to contribute substantially to an improved mechanistic understanding of viral infection, cellular production and release, and hence highly facilitate the development of novel approaches to prevention and therapy. Furthermore, it is anticipated that they will complement present techniques of electron microscopy and molecular biology to identify viruses in specific infected cells, e.g., inside tissue sections; eventually, COMBO-FISH-based multicolor localization microscopy techniques might even be used to detect, identify and count viruses at 'hot spots' in the environment (e.g., in a hospital, in sites open to the public, or in food), as an alternative to PCR techniques. Finally, they are ideally suited to promote the development of virus-scaffolded multifunctional nanomaterials and devices, for which numerous fields of applications are arising.

Acknowledgments The generous supports of the Boehringer Ingelheim Foundation to C.C., of the Deutsche Forschungsgemeinschaft (German Research Council) to C.C. and C.W., and of the Bundesministerium für Bildung und Forschung (Federal Ministry for Education and Research) to M.H. and the Baden-Wuerttemberg-Stiftung to C.W. are gratefully acknowledged. For support in some of the localization microscopy measurements we thank Qiao Wang and Sebastian Pres, and for critical reading of the manuscript Prof. Christina Ehrhard, Institute of Molecular Virology University Münster, Germany. The authors also thank Dr. Niels Lemmermann and Prof. Rafaela Holtappels, Institute of Virology, University Medical Center Mainz for providing the specimens of gp36.5/m164.

References

Abbe E (1873) Beiträge zur Theorie des Mikroskops und der mikroskopischen Wahrnehmung. Arch Für Mikrosk Anat 9:413–418

Albrecht B, Failla AV, Heintzmann R, Cremer C (2001) Spatially modulated illumination microscopy: online visualization of intensity distribution and prediction of nanometer precision of axial distance measurements by computer simulations. J Biomed Opt 6:292–299. doi:10.1117/1.1383293

Albrecht B, Failla AV, Schweitzer A, Cremer C (2002) Spatially modulated illumination microscopy allows axial distance resolution in the nanometer range. Appl Opt 41:80–87

Alonso JM, Górzny MŁ, Bittner AM (2013) The physics of tobacco mosaic virus and virus-based devices in biotechnology. Trends Biotechnol 31:530–538

Atanasova P, Rothenstein D, Schneider JJ, Hoffmann RC, Dilfer S, Eiben S, Wege C, Jeske H, Bill J (2011) Virus-templated synthesis of ZnO nanostructures and formation of field-effect transistors. Adv Mat 23:4918–4922

Azucena C, Eber FJ, Trouillet V, Hirtz M, Heissler S, Franzreb M, Fuchs H, Wege C, Gliemann H (2012) New approaches for bottom-up assembly of tobacco mosaic virus-derived nucleoprotein tubes on defined patterns on silica- and polymer- based substrates. Langmuir 28:14867–14877

Baddeley D, Batram C, Weiland Y, Cremer C, Birk UJ (2007) Nanostructure analysis using spatially modulated illumination microscopy. Nat Protoc 2:2640–2646. doi:10.1038/nprot.2007.399

Baddeley D, Jayasinghe ID, Cremer C, Cannell MB, Soeller C (2009) Light-induced dark states of organic fluochromes enable 30 nm resolution imaging in standard media. Biophys J 96:L22–L24. doi:10.1016/j.bpj.2008.11.002

Baddeley D, Chagin VO, Schermelleh L, Martin S, Pombo A, Carlton PM, Gahl A, Domaing P, Birk U, Leonhardt H, Cremer C, Cardoso MC (2010) Measurement of replication structures at the nanometer scale using super-resolution light microscopy. Nucleic Acids Res 38:e8. doi:10.1093/nar/gkp901

Baddeley D, Crossman D, Rossberger S, Cheyne JE, Montgomery JM, Jayasinghe ID, Cremer C, Cannell MB, Soeller C (2011) 4D super-resolution microscopy with conventional fluorophores and single wavelength excitation in optically thick cells and tissues. PLoS ONE 6:e20645. doi:10.1371/journal.pone.0020645

Bates M, Huang B, Dempsey GT, Zhuang X (2007) Multicolor super-resolution imaging with photo-switchable fluorescent probes. Science 317:1749–1753. doi:10.1126/science.1146598

Beliveau BJ, Joyce EF, Apostolopoulos N, Yilmaz F, Fonseka CY, McCole RB, Chang Y, Li JB, Senaratne TN, Williams BR, Rouillard J-M, Wu C (2012) Versatile design and synthesis platform for visualizing genomes with Oligopaint FISH probes. Proc Natl Acad Sci 201213818. doi:10.1073/pnas.1213818110

Betzig E (1995) Proposed method for molecular optical imaging. Opt Lett 20:237–239

Betzig E, Patterson GH, Sougrat R, Lindwasser OW, Olenych S, Bonifacino JS, Davidson MW, Lippincott-Schwartz J, Hess HF (2006) Imaging intracellular fluorescent proteins at nanometer resolution. Science 313:1642–1645. doi:10.1126/science.1127344

Bittner AM, Alonso JM, Górzny ML, Wege C (2013) Nanoscale science and technology with plant viruses and bacteriophages. In: Mateu MG (ed) Structure and physics of viruses: an integrated textbook, pp 667–702. Dordrecht: Springer Science + Business Media. ISBN 978-94-007-6551-1. Series: Subcellular Biochemistry (Harris, J.R., Series ed.), ISSN: 0306-0225

Blum AS, Soto CM, Sapsford KE, Wilson CD, Moore MH, Ratna BR (2011) Molecular electronics based nanosensors on a viral scaffold. Biosens Bioelectron 26:2852–2857

Bock H, Geisler C, Wurm CA, Von Middendorff C, Jakobs S, Schönle A, Egner A, Hell SW, Eggeling C (2007) Two-color far-field fluorescence nanoscopy based on photoswitchable emitters. Appl Phys B 88:161–165

Bolzer A, Kreth G, Solovei I, Koehler D, Saracoglu K, Fauth C, Müller S, Eils R, Cremer C, Speicher MR, Cremer T (2005) Three-Dimensional Maps of All Chromosomes in Human Male Fibroblast Nuclei and Prometaphase Rosettes. Public Library of Science (PloS) 3:826–842

Bornfleth H, Saetzler K, Eils R, Cremer C (1998) High-precision distance measurements and volume-conserving segmentation of objects near and below the resolution limit in three-dimensional confocal fluorescence microscopy. J Microsc 189:118–136

Bottaro DP, Rubin JS, Faletto DL, Chan AM, Kmiecik TE, Woude GV, Aaronson SA (1991) Identification of the hepatocyte growth factor receptor as the c-met proto-oncogene product. Science 251:802–804

Bruckman MA, Hern S, Jiang K, Flask CA, Yu X, Steinmetz NF (2013) Tobacco mosaic virus rods and spheres as supramolecular high-relaxivity MRI contrast agents. J Mater Chem B 1:1482–1490

Cardinale D, Carette N, Michon T (2012) Virus scaffolds as enzyme nano-carriers. Trends Biotechnol 30:369–376

Chojnacki J, Staudt T, Glass B, Bingen P, Engelhardt J, Anders M, Schneider J, Müller B, Hell SW, Kräusslich H-G (2012) Maturation-Dependent HIV-1 Surface Protein Redistribution Revealed by Fluorescence Nanoscopy. Science 338:524–528. doi:10.1126/science.1226359

Cooper CS (1992) The met oncogene: from detection by transfection to transmembrane receptor for hepatocyte growth factor. Oncogene 7:3–7

Cremer C (2012) Optics far beyond the diffraction limit. Springer Handb. Lasers Opt. Springer, pp 1359–1397

Cremer T, Cremer C (2001) Chromosome territories and the functional nuclear architecture. Nat Rev 2:292–301

Cremer C, Masters BR (2013) Resolution enhancement techniques in microscopy. Eur Phys J H 38:281–344. doi:10.1140/epjh/e2012-20060-1

Cremer C, Hausmann M, Bradl C, Rinke B (1998) Method and devices for measuring distances between object structures. German Patent (filing date 23 Dec 1996) 196.54.824.1/DE, 23 Jul 2002; European Patent EP 0 946 855 B1/Oct 17, 2001

Cremer C, Edelmann P, Bornfleth H, Kreth G, Muench H, Luz H, Hausmann M (1999) Principles of spectral precision distance confocal microscopy for the analysis of molecular nuclear structure. Handb Comput Vis Appl Syst Appl, 1st ed. Academic Press, San Diego, pp 839–857

Cremer C, Failla AV, Albrecht B (2003) Far field light microscopical method, system and computer program product for analysing at least one object having a subwavelength size. US Patent 7,298,461 B2/Nov. 20, 2007 (publ. April 17, 2003)

Cremer C, Kaufmann R, Gunkel M, Pres S, Weiland Y, Müller P, Ruckelshausen T, Lemmer P, Geiger F, Degenhard S, Wege C, Lemmermann NAW, Holtappels R, Strickfaden H, Hausmann M (2011) Superresolution imaging of biological nanostructures by spectral precision distance microscopy. Biotechnol J 6:1037–1051. doi:10.1002/biot.201100031

Däubner T, Fink A, Seitz A, Tenzer S, Müller J, Strand D, Seckert CK, Janssen C, Renzaho A, Grzimek NKA, Simon CO, Ebert S, Reddehase MJ, Oehrlein-Karpi SA, Lemmermann NAW (2010) A novel transmembrane domain mediating retention of a highly motile herpesvirus glycoprotein in the endoplasmic reticulum. J Gen Virol 91:1524–1534. doi:10.1099/vir.0.018580-0

Dempsey GT, Vaughan JC, Chen KH, Bates M, Zhuang X (2011) Evaluation of fluorophores for optimal performance in localization-based super-resolution imaging. Nat Methods 8:1027–1036. doi:10.1038/nmeth.1768

Donnert G, Keller J, Medda R, Andrei MA, Rizzoli SO, Lührmann R, Jahn R, Eggeling C, Hell SW (2006) Macromolecular-scale resolution in biological fluorescence microscopy. Proc Natl Acad Sci 103:11440–11445. doi:10.1073/pnas.0604965103

Eber FJ, Eiben S, Jeske H, Wege C (2013) Bottom-up-assembled nanostar colloids of gold cores and tubes derived from tobacco mosaic virus. Angew Chem Int Ed 52:7203–7207

Eiben S, Stitz N, Eber F, Wagner J, Atanasova P, Bill J, Wege C, Jeske H (2014) Tailoring the surface properties of tobacco mosaic virions by the integration of bacterially expressed mutant coat protein. Virus Res 180:92–96

Eierhoff T, Hrincius ER, Rescher U, Ludwig S, Ehrhardt C (2010) The Epidermal Growth Factor Receptor (EGFR) Promotes Uptake of Influenza A Viruses (IAV) into Host Cells. PLoS Pathog 6:e1001099. doi:10.1371/journal.ppat.1001099

Esa A, Edelmann P, Kreth G, Trakhtenbrot L, Amariglio N, Rechavi G, Hausmann M, Cremer C (2000) Three-dimensional spectral precision distance microscopy of chromatin nanostructures after triple-colour DNA labelling: a study of the BCR region on chromosome 22 and the Philadelphia chromosome. J Microsc 199:96–105

Esa A, Coleman AE, Edelmann P, Silva S, Cremer C, Janz S (2001) Conformational differences in the 3D-nanostructure of the immunoglobulin heavy-chain locus, a hotspot of chromosomal translocations in B lymphocytes. Cancer Genet Cytogenet 127:168–173

Fölling J, Bossi M, Bock H, Medda R, Wurm CA, Hein B, Jakobs S, Eggeling C, Hell SW (2008) Fluorescence nanoscopy by ground-state depletion and single-molecule return. Nat Methods 5:943–945. doi:10.1038/nmeth.1257

Galland F, Stefanova M, Lafage M, Birnbaum D (1992) Localization of the 5′ end of the MCF2 oncogene to human chromosome 15q15—q23. Cytogenet Cell Genet 60:114–116

Geiger FC, Eber FJ, Eiben S, Mueller A, Jeske H, Spatz JP, Wege C (2013) TMV nanorods with programmed longitudinal domains of differently addressable coat proteins. Nanoscale 5:3808–3816

Grossmann C, Schwarz-Finsterle J, Schmitt E, Birk U, Hildenbrand G, Cremer C, Trakhtenbrot L, Hausmann M (2010) Variations of the spatial fluorescence distribution in ABL gene chromatin domains measured in blood cell nuclei by SMI microscopy after COMBO–FISH labelling. In: Méndez-Vilas A, Díaz Álvarez J (eds) Microscopy: science, technology, applications and education vol. 1, pp 688–695

Gunkel M (2011) Lokalisationsmikroskopie mit mehreren Farben und ihre Anwendung in biologischen Präparaten (localization microscopy with several colors and its application to biological specimens). Ph.D. Thesis (Physics), University Bielefeld/Germany

Gunkel M, Erdel F, Rippe K, Lemmer P, Kaufmann R, Hörmann C, Amberger R, Cremer C (2009) Dual color localization microscopy of cellular nanostructures. Biotechnol J 4:927–938. doi:10.1002/biot.200900005

Gustafsson MG (2000) Surpassing the lateral resolution limit by a factor of two using structured illumination microscopy. J Microsc 198:82–87

Ha T, Enderle T, Chemla DS, Weiss S (1996) Dual-molecule spectroscopy: molecular rulers for the study of biological macromolecules. IEEE J Sel Top Quantum Electron 2:1115–1128

Harder A, Dieding M, Walhorn V, Degenhard S, Brodehl A, Wege C, Milting H, Anselmetti D (2013) Apertureless scanning near-field optical microscopy of sparsely labelled tobacco mosaic viruses and intermediate filament desmin. Beilstein J. Nanotechnol. 4:510–516

Hausmann M, Winkler R, Hildenbrand G, Finsterle J, Weisel A, Rapp A, Schmitt E, Janz S, Cremer C (2003) COMBO-FISH: specific labeling of nondenatured chromatin targets by computer-selected DNA oligonucleotide probe combinations. Biotechniques 35:564–577

Heilemann M, Herten DP, Heintzmann R, Cremer C, Müller C, Tinnefeld P, Weston KD, Wolfrum J, Sauer M (2002) High-resolution colocalization of single dye molecules by fluorescence lifetime imaging microscopy. Anal Chem 74:3511–3517

Heilemann M, van de Linde S, Schüttpelz M, Kasper R, Seefeldt B, Mukherjee A, Tinnefeld P, Sauer M (2008) Subdiffraction-resolution fluorescence imaging with conventional fluorescent probes. Angew Chem Int Ed 47:6172–6176

Heintzmann R, Cremer CG (1999) Laterally modulated excitation microscopy: improvement of resolution by using a diffraction grating. Proc. SPIE 3568:185–196

Heintzmann R, Gustafsson MGL (2009) Subdiffraction resolution in continuous samples. Nat Photonics 3:362–364. doi:10.1038/nphoton.2009.102

Hell SW (2007) Far-field optical nanoscopy. Science 316:1153–1158

Hell SW (2009) Microscopy and its focal switch. Nat Methods 6:24–32. doi:10.1038/nmeth.1291

Herzenberg LA, Parks D, Sahaf B, Perez O, Roederer M, Herzenberg LA (2002) The History and Future of the Fluorescence Activated Cell Sorter and Flow Cytometry: A View from Stanford. Clin Chem 48:1819–1827

Hess ST, Girirajan TP, Mason MD (2006) Ultra-high resolution imaging by fluorescence photoactivation localization microscopy. Biophys J 91:4258–4272

Hess ST, Gould TJ, Gunewardene M, Bewersdorf J, Mason MD (2009) Ultrahigh Resolution Imaging of Biomolecules by Fluorescence Photoactivation Localization Microscopy. In: Foote RS, Lee JW (eds) Micro Nano Technol. Humana Press, Bioanal, pp 483–522

Hildenbrand G, Rapp A, Spöri U, Wagner C, Cremer C, Hausmann M (2005) Nano-sizing of specific gene domains in intact human cell nuclei by spatially modulated illumination light microscopy. Biophys J 88:4312–4318

Holtappels R, Grzimek NKA, Simon CO, Thomas D, Dreis D, Reddehase MJ (2002a) Processing and presentation of murine cytomegalovirus pORFm164-derived peptide in fibroblasts in the face of all viral immunosubversive early gene functions. J Virol 76:6044–6053

Holtappels R, Thomas D, Podlech J, Reddehase MJ (2002b) Two Antigenic Peptides from Genes m123 and m164 of Murine Cytomegalovirus Quantitatively Dominate CD8 T- Cell Memory in the H-2d Haplotype. J Virol 76:151–164. doi:10.1128/JVI.76.1.151-164.2002

Huang B, Wang W, Bates M, Zhuang X (2008) Three-dimensional super-resolution imaging by stochastic optical reconstruction microscopy. Science 319:810–813

Huber O, Brunner A, Maier P, Kaufmann R, Couraud P-O, Cremer C, Fricker G (2012) Localization microscopy (SPDM) reveals clustered formations of P-glycoprotein in a human blood-brain barrier model. PLoS ONE 7:e44776. doi:10.1371/journal.pone.0044776

Kadri A, Maiss E, Amsharov N, Bittner A, Balci S, Kern K, Jeske H, Wege C (2011) Engineered tobacco mosaic virus mutants with distinct physical characteristics in planta and enhanced metallization properties. Virus Res 157:35–46

Kaufmann R, Lemmer P, Gunkel M, Weiland Y, Müller P, Hausmann M, Baddeley D, Amberger R, Cremer C (2009) SPDM: single molecule superresolution of cellular nanostructures. Proc. SPIE 7185:71850J-1–71850J-19

Kaufmann R, Müller P, Hildenbrand G, Hausmann M, Cremer C (2011) Analysis of Her2/neu membrane protein clusters in different types of breast cancer cells using localization microscopy. J Microsc 242:46–54. doi:10.1111/j.1365-2818.2010.03436.x

Kaufmann R, Piontek J, Grüll F, Kirchgessner M, Rossa J, Wolburg H, Blasig IE, Cremer C (2012) Visualization and quantitative analysis of reconstituted tight junctions using localization microscopy. PLoS ONE 7:e31128. doi:10.1371/journal.pone.0031128

Lee S-Y, Lim J-S, Harris MT (2012) Synthesis and application of virus-based hybrid nanomaterials. Biotechnol Bioeng 109:16–30

Lemmer P, Gunkel M, Baddeley D, Kaufmann R, Urich A, Weiland Y, Reymann J, Müller P, Hausmann M, Cremer C (2008) SPDM: light microscopy with single-molecule resolution at the nanoscale. Appl Phys B 93:1–12

Lemmer P, Gunkel M, Weiland Y, Müller P, Baddeley D, Kaufmann R, Urich A, Eipel H, Amberger R, Hausmann M, Cremer C (2009) Using conventional fluorescent markers for far-field fluorescence localization nanoscopy allows resolution in the 10-nm range. J Microsc 235:163–171. doi:10.1111/j.1365-2818.2009.03196.x

Lidke KA, Rieger B, Jovin TM, Heintzmann R (2005) Superresolution by localization of quantum dots using blinking statistics. Opt Express 13:7052–7062

Löschberger A, van de Linde S, Dabauvalle M-C, Rieger B, Heilemann M, Krohne G, Sauer M (2012) Super-resolution imaging visualizes the eightfold symmetry of gp210 proteins around the nuclear pore complex and resolves the central channel with nanometer resolution. J Cell Sci 125:570–575

Mueller A, Kadri A, Jeske H, Wege C (2010) In vitro assembly of Tobacco mosaic virus coat protein variants derived from fission yeast expression clones or plants. J Virol Methods 166:77–85. doi:10.1016/j.jviromet.2010.02.026

Mueller A, Eber FJ, Azucena C, Petershans A, Bittner AM, Gliemann H, Jeske H, Wege C (2011) Inducible site-selective bottom-up assembly of virus-derived nanotube arrays on RNAequipped wafers. ACS Nano 5:4512–4520

Müller P, Schmitt E, Jacob A, Hoheisel J, Kaufmann R, Cremer C, Hausmann M (2010) COMBO-FISH Enables High Precision Localization Microscopy as a Prerequisite for Nanostructure Analysis of Genome Loci. Int J Mol Sci 11:4094–4105. doi:10.3390/ijms11104094

Müller P, Weiland Y, Kaufmann R, Gunkel M, Hillebrandt G, Cremer C, Hausmann M (2012) Analysis of fluorescent nanostructures in biological systems by means of spectral position determination microscopy (SPDM). In Méndez-Vilas A (ed) Current microscopy contributions to advances in science and technology vol. 1, pp 3–12

Müller P, Lemmermann NAW, Kaufmann R, Gunkel M, Paech D, Hildenbrand G, Birk U, Holtappels R, Cremer C, Hausmann M (2014) Spatial distribution and structural arrangement of a murine cytomegalovirus glycoprotein detected by SPDM localization microscopy. Histochem Cytochem

Muranyi W, Malkusch S, Müller B, Heilemann M, Kräusslich H-G (2013) Super-Resolution Microscopy Reveals Specific Recruitment of HIV-1 Envelope Proteins to Viral Assembly Sites Dependent on the Envelope C-Terminal Tail. PLoS Pathog 9:e1003198. doi:10.1371/journal.ppat.1003198

Pertsinidis A, Zhang Y, Chu S (2010) Subnanometre single-molecule localization, registration and distance measurements. Nature 466:647–651

Rauch J, Hausmann M, Solovei I, Horsthemke B, Cremer T, Cremer C (2000) Measurement of local chromatin compaction by spectral precision distance microscopy. Proc SPIE 4164:1–9

Rauch J, Knoch TA, Solovei I, Teller K, Stein S, Buiting K, Horsthemke B, Langowski J, Cremer T, Hausmann M, Cremer C (2008) Lightoptical precision measurements of the active and inactive Prader-Willi Syndrome imprinted regions in human cell nuclei. Differentiation 76:66–82

Rayleigh Lord (1896) On the theory of optical images, with special reference to the microscope. Philos Mag J Sci 42:167–195

Reymann J, Baddeley D, Gunkel M, Lemmer P, Stadter W, Jegou T, Rippe K, Cremer C, Birk U (2008) High-precision structural analysis of subnuclear complexes in fixed and live cells via spatially modulated illumination (SMI) microscopy. Chromosome Res 16:367–382. doi:10.1007/s10577-008-1238-2

Rust MJ, Bates M, Zhuang X (2006) Sub-diffraction-limit imaging by stochastic optical reconstruction microscopy (STORM). Nat Methods 3:793–796

Schermelleh L, Carlton PM, Haase S, Shao L, Winoto L, Kner P, Burke B, Cardoso MC, Agard DA, Gustafsson MGL, Leonhardt H, Sedat JW (2008) Subdiffraction multicolor imaging of the nuclear periphery with 3D structured illumination microscopy. Science 320:1332–1336. doi:10.1126/science.1156947

Schmidt M, Nagorny M, Hell SW (2000) Subresolution axial measurements in far-field fluorescence microscopy with precision of 1 nanometer. Rev Sci Instr 71:2742–2745

Shroff H, Galbraith CG, Galbraith JA, Betzig E (2008) Live-cell photoactivated localization microscopy of nanoscale adhesion dynamics. Nat Methods 5:417–423

Shtengel G, Galbraith JA, Galbraith CG, Lippincott-Schwartz J, Gillette JM, Manley S, Sougrat R, Waterman CM, Kanchanawong P, Davidson MW (2009) Interferometric fluorescent super-resolution microscopy resolves 3D cellular ultrastructure. Proc Natl Acad Sci 106:3125–3130

Spicuzza L, Spicuzza A, La Rosa M, Polosa R, Di Maria G (2007) New and emerging infectious diseases. Allergy Asthma Proc 28:28–34

Steinhauer C, Forthmann C, Vogelsang J, Tinnefeld P (2008) Super-resolution Microscopy on the Basis of Engineered Dark States. J Am Chem Soc 130:16840–16841. doi:10.1021/ja806590m

Steinmetz NF, Manchester M (2011) Viral nanoparticles – tools for materials science and biomedicine. Pan Stanford Publishing, Singapore

Swayne D, Halvorson D (2008) Influenza. Dis. Poult., 12th ed. Wiley, pp 153–184

Van de Linde S, Löschberger A, Klein T, Heidbreder M, Wolter S, Heilemann M, Sauer M (2011) Direct stochastic optical reconstruction microscopy with standard fluorescent probes. Nature Protoc 6:991–1009

Van Oijen AM, Köhler J, Schmidt J, Müller M, Brakenhoff GJ (1998) 3-Dimensional super- resolution by spectrally selective imaging. Chem Phys Lett 292:183–187

Wang Q, Dierkes R, Kaufmann R, Cremer C (2014) Quantitative analysis of individual hepatocyte growth factor receptor clusters in influenza A virus infected human epithelial cells using localization microscopy. Biochim Biophys Acta. doi:10.1016/j.bbamem.2013.12.014

Weidner KM, Sachs M, Birchmeier W (1993) The Met receptor tyrosine kinase transduces motility, proliferation, and morphogenic signals of scatter factor/hepatocyte growth factor in epithelial cells. J Cell Biol 121:145–154

Weiland Y, Lemmer P, Cremer C (2011) Combining FISH with localisation microscopy: Super-resolution imaging of nuclear genome nanostructures. Chromosome Res 19:5–23. doi:10.1007/s10577-010-9171-6

Wu Z, Mueller A, Degenhard S, Ruff SE, Geiger F, Bittner A, Wege C, Krill C III (2010) Enhancing the magnetoviscosity of ferrofluids by the addition of biological nanotubes. ACS Nano 4:4531–4538

Zhuang X (2009) Nano-imaging with Storm. Nat Photonics 3:365–367. doi:10.1038/nphoton.2009.101

Zwick E, Bange J, Ullrich A (2001) Receptor tyrosine kinase signalling as a target for cancer intervention strategies. Endocr Relat Cancer 8:161–173